Separation and Purification Technology 398 (2026) 138152

Contents lists available at ScienceDirect

Separation and Purification Technology

journal homepage: www.elsevier.com/locate/seppur

An ambient aqueous route to scalable ZIF-8 fabrics for harmful gas capture

Huailing Diao [a], Shuo Shi [a], Kaikai Ma [b,*], Han Li [a], Yumeng Tang [c], Jinfeng Wang [c], Qingtao Liu [c], Xungai Wang [d,*]

[a] Joint Research Centre for Fiber Innovations and Renewable Materials (JRC-FIRM), School of Fashion and Textiles, The Hong Kong Polytechnic University, Hung Hom, Hong Kong Special Administrative Region of China

[b] Research Institute for Intelligent Wearable Systems, School of Fashion and Textiles, The Hong Kong Polytechnic University, Hung Hom, Hong Kong Special Administrative Region of China

[c] National Local Joint Engineering Laboratory for Advanced Textile Processing and Clean Production, Wuhan Textile University, Wuhan, China

[d] State Key Laboratory of Bio-based Fiber Materials, College of Textile Science and Engineering, Zhejiang Sci-Tech University, Hangzhou, China

ARTICLE INFO

Editor name:

Keywords:
Zeolitic imidazolate frameworks
Ambient aqueous synthesis
Fabric substrate
Self-sacrificial ZnO templating
Harmful gas adsorption

ABSTRACT

Removing specific environmental and harmful contaminants presents a significant technological challenge. While zeolitic imidazolate framework-8 (ZIF-8) in powder form has excellent gas adsorption capacity and stability, developing an eco-friendly method to effectively incorporate the ZIF-8 powder into flexible substrates is crucial for its practical applications. Herein, we propose a solid-state method to prepare self-sacrificial ZnO template, and then convert the template into ZIF-8 coating on fabrics in an ambient aqueous solution. The randomly aligned ZnO nanorods on fabric surfaces serve as both sacrificial templates and nucleation sites, and the solid-liquid interfacial coordination between Zn^{2+} released from ZnO and 2-methylimidazole aqueous solution enabled rapid formation of a dense ZIF-8 intergrown coating with tunable size and loading content. The mechanism of the transformation from solid precursor to crystalline ZIF-8 coating was inferred. The coated fabrics featured outstanding stability and easy processability. Furthermore, the porous fabric showed high adsorption capability, stability and recyclability for ammonia. This inexpensive, controllable and scalable method for synthesizing ZIF-8 coatings in an ambient aqueous solution offers a feasible route for the applications of human health and environmental sustainability.

1. Introduction

In recent years, the environmental and health risks associated with harmful gases have attracted significant global attention, driving the development of high-performance gas adsorbent materials such as metal-organic frameworks (MOFs) [1–7]. Among these materials, zeolitic imidazolate framework-8 (ZIF-8) has demonstrated exceptional gas adsorption potential owing to its high specific surface area, microporous structure and excellent chemical stability [8,9]. However, utilizing ZIF-8 in powder form remains difficult due to its poor processability and tendency to agglomerate. Developing a controllable and eco-friendly method to integrate ZIF-8 powder effectively into flexible substrates is crucial for practical applications. [10–12]. Flexible fabric substrates, featuring a porous structure, inherent breathability, and wearability advantages, have emerged as an ideal platform for functional integration of ZIF-8 [11,13–16].

ZIF-8 is formed by the combination of a Zn^{2+} source with 2-methylimidazole (2-MIM) in a suitable solvent and crystallizes in a sodalite structure [17,18]. Conventional solvothermal methods for the direct solution synthesis of ZIF-8 on fabric surfaces face multiple challenges, such as insufficient crystal nucleation sites leading to low loading efficiency, inhomogeneous crystal distribution, and weak interfacial bonding [19,20]. Some researchers have introduced reactive functional groups (e.g., carboxyl groups) onto substrate surfaces to provide more nucleation sites [14,21]. However, this chemical modification of a substrate involves a complex process, and even after modification, the mass loading capacity still remains relatively low.

Existing improvement strategies focus on the utility of a prefabricated ZnO or Zn-based solid precursor as a sacrificial template and a Zn^{2+} source for in-situ ZIF-8 formation [15,17,19,22]. In the first step, there are various methods to prepare ZnO or Zn-based solid precursor on the surface of substrate, such as atomic layer deposition (ALD) [23,24], sol-gel coating [25] and hydrothermal method [19,26], which are typically applied on inorganic substrates. Actually, ALD represents a

* Corresponding authors.
E-mail addresses: kaikai.ma@polyu.edu.hk (K. Ma), xwang@zstu.edu.cn (X. Wang).

https://doi.org/10.1016/j.seppur.2026.138152
Received 10 March 2026; Received in revised form 14 April 2026; Accepted 21 April 2026
Available online 22 April 2026

high-cost thin-film deposition technique that requires expensive precursors, high-vacuum equipment, and extended deposition times, and the thin ZnO film results in low ZIF-8 loading after conversion [24]. Regarding Zn-based sol-gel coating, it is difficult to apply the gel evenly on the substrate surface. Moreover, the subsequent conversion into ZIF-8 requires an autoclave and high-temperature, high-pressure conditions to facilitate vapor deposition [25]. The hydrothermal method for preparing ZnO coating is typically completed in the Teflon-lined stainless-steel autoclave and involves high temperatures and long reaction times [19,20,26–28]. Therefore, these high-energy methods that require harsh conditions are typically restricted to inorganic substrates, which limits their application to fabrics. In the second step of the conversion of ZnO to ZIF-8, most solution synthesis methods require large amounts of organic solvents such as methanol [29,30], ethanol [15] and *N*, *N*-dimethylformamide (DMF) [22,26], making them environmentally unfriendly. Besides solution synthesis of ZIF-8 coating, mechanochemical coating without solvent is also used, which includes roll-to-roll hot-pressing process and ball milling [31,32]. However, these mechanochemical methods involve heat and pressure, which results in high energy consumption, and is not suitable for practical production.

In this study, we propose a solid-state method to prepare self-sacrificial ZnO template, and then convert the template into ZIF-8 coating on fabrics in an ambient aqueous solution. ZnO nanorods grew evenly on the surface of fabrics through regulating the liquid precursor concentration, which served as a template for the solid precursor and subsequent nucleation site for controlled ZIF-8 growth. When the ZnO coated fabric material was treated with the linker, a rapid coordination reaction occurred at the interfacial layer between the solid precursor and the ligand solution to form amorphous precursor intermediates, which subsequently transformed into the dense ZIF-8 crystals with controllable size and content. The mechanical strength, laundering durability, moisture permeability and hydrophobicity character of large-scaled ZIF-8-loaded fabrics were systematically evaluated. Furthermore, a series of fabrics coated with ZIF-8 were engineered to systematically investigate their adsorption capacity and kinetic toward representative harmful gases, including ammiona (NH_3), acetic acid (CH_3COOH) and carbon dioxide (CO_2) gaseous compounds.

2. Experimental section

2.1. Materials

A cotton fabric with an areal density of 277 g m^{-2}, a polyester fabric with an areal density of 200 g m^{-2} and a flax fabric with an areal density of 154 g m^{-2} were provided by China Dye Ltd., Hong Kong. Zinc acetate dihydrate (≥99.0%), 2-methylimidazole (≥99.0%), methanol (≥99.8%) and ethanol (≥99.8%) were purchased from Dieckmann.

2.2. Preparations of self-sacrificial ZnO templating

Ten pieces of cotton fabrics (5 cm × 5 cm) were immersed in 100 mL of a zinc acetate dihydrate aqueous solution with a weight concentration of 5, 10, 20 and 30% for 2 h. After the removal from the bath solution, the fabrics were rolled through a laboratory padder at a nip pressure of 4 kg cm^{-2} with a rotation speed of 5 rpm for two cycles to remove excess liquid and make the remaining liquid more uniform. Then dried at 130 °C for 2 h to form the ZnO coated fabrics. After washing with deionized water, the ZnO coated fabrics were dried in air at room temperature.

2.3. Fabrication of ZIF-8 coating on the cotton textile

The ZnO coated cotton fabric samples were immersed in 100 mL of a 2 M 2-MIM water solution for 4 h. Then solution and textiles were washed by water and methanol for four times using centrifuge at 10000 rpm. Then the ZIF-8 coating textiles and ZIF-8 powders were dried in air at room temperature.

2.4. Characterization

The morphologies and microstructures of the samples were examined using a TESCAN MAIA3 field emission scanning electron microscope (SEM) on gold sputter coated samples. Energy dispersive X-ray analysis (EDS) was also carried out along with SEM. Powder X-ray diffraction (PXRD) was recorded in the reflection mode in the angular range of 5–40° (2θ) with a scanning speed of 5°/min by using an X-ray diffractometer (Rigaku SmartLab 9 kW-Advance), and the wavelength of the Cu Kα radiation source was 1.54 Å. Attenuated total reflectance Fourier transform infrared (ATR-FTIR) spectra of all samples were recorded using Bruker, ALPHA Germany spectrometer in the range from 550 to 4000 cm^{-1} at 4 cm^{-1} resolution and 16 scans. Thermogravimetric analyses (TGA) were performed on TGA8000 from 30 °C to 800 °C with a heating rate of 10 °C min^{-1} in air atmosphere. Scienta Omicron X-ray photoelectron spectroscopy (XPS) was used to examine the surface chemistry using monochromatic aluminum K-rays with photon energies of 1486.7 eV. The breaking strength and elongation of the textile samples along the longitudinal and latitudinal direction were tested according to a grab test method [ASTM D5034–09 (2017)] on a tensile strength tester (Instron 4411). Five replicates were tested for the breaking strength and breaking elongation, and the average values were reported. Static water contact angles (WCA) were measure, and data was acquired for a 5 s period after initial impingement. Water vapor permeability testing was done using a modified BS7209 method. Wash durability was evaluated at 50 °C with the equivalent of 4 g/500 mL ECE Phosphate Reference Detergent (SDC Type 3) in water for 40 min in a Launder-O-meter (Atlas, USA). Nitrogen (N_2) adsorption-desorption isotherms and Brunauer-Emmett-Teller (BET) surface area data were collected on Micromeritics ASAP 2020 Micropore Analyzer at 77 K, and carbon dioxide (CO_2) adsorption-desorption isotherms were recorded at 298 K.

2.5. Gas adsorption and kinetic adsorption models

Dynamic monitoring of acetic acid and ammonia adsorption was carried out in an air-tight odor detection system with a determined volume (12 μL) of acetic acid and ammonia solution for the samples (2.0 g). To transparently define the environmental tolerance of our composite, we clarify that all adsorption and stability tests were conducted under challenging ambient conditions (25 °C and 63% relative humidity). The concentration of adsorbed gas onto adsorbent at any time (q_t) was calculated by Eq. 1.

$$q_t = \frac{(C_0 - C_t)V}{M} \tag{1}$$

where C_0 and C_t are the initial concentration (mg·L^{-1}) and real-time concentration (mg·L^{-1}) of gas, respectively, q_t is the real-time concentration of gas adsorbed onto adsorbents, which is also called as the adsorption capacity (mg·g^{-1}), V is the volume of the sample chamber (4.5 L), and M is the mass of adsorbents used for each test (2.0 g).

Adsorption kinetics provide important parameters such as adsorption rate constants to assess adsorption mechanisms and efficiency while predicting experimental results. The adsorption process typically involved three sequential stages: external mass transfer, intra-particle diffusion, and adsorption reaction. Diffusion dynamics were analyzed using Dunwald-Wagner (D—W) and Weber-Morris (W-M) models, while pseudo-first-order (PFO) and pseudo-second-order (PSO) kinetic models described the reaction mechanism [33,34].

The D—W model is presented by Eq. 2 and 3.

$$log(1 - F^2) = -\frac{k}{2.303}t \tag{2}$$

$$F = \frac{q_t}{q_e} \tag{3}$$

where k is the diffusion rate constant (min^{-1}), which can be obtained by plotting log ($1\text{-}F^2$) against t. q_t ($mg{\cdot}g^{-1}$) and q_e ($mg{\cdot}g^{-1}$) are the odor adsorption quantity of samples at contact time and at equilibrium, respectively. F is the odor removal percent calculated by q_t/q_e.

The W-M model is commonly applied to describe the intraparticle diffusion process which was presented by Eq. 4.

$$q_t = k_{id}t^{1/2} + C \tag{4}$$

where k_{id} ($mg{\cdot}g^{-1}{\cdot}min^{-1/2}$) is the intra-particle diffusion rate constant, C is the boundary layer thickness. The rate constant k_{id} and C can be obtained by plotting q_t against $t^{1/2}$.

The PFO model is presented by Eq. 5.

$$\ln(q_e - q_t) = \ln q_e - k_1 t \tag{5}$$

where q_e ($mg{\cdot}g^{-1}$) is the equilibrium adsorption quantity obtained by PFO model. The rate constant (k_1) is the PFO rate constant (min^{-1}). k_1 and q_e were calculated from the slope and intercept of the plot of ln (q_e–q_t) against t.

The PSO model is presented by Eq. 6 and 7.

$$\frac{t}{q_t} = \frac{1}{k_2 q_e^2} + \frac{t}{q_e} \tag{6}$$

$$h_2 = k_2 q_e^2 \tag{7}$$

where q_e ($mg{\cdot}g^{-1}$) is the equilibrium adsorption quantity calculated by PSO model. k_2 is the PSO rate constant ($g{\cdot}mg1{\cdot}min^{-1}$), which is used to describe the rate of adsorption equilibrium. The equilibrium adsorption quantity (q_e) and the rate constant (k_2) can be calculated from the slope and intercept of the plot of t/q_t versus t.

3. Results and discussion

3.1. Fabrication of ZIF-8 coated fabrics via self-sacrificial ZnO templating

To fabricate the ZIF-8 coated fabric through ZnO self-templating, a ZnO layer was initially deposited on the fabric by immersing it in zinc acetate dihydrate ($Zn(CH_3COO)_2$) aqueous solution followed by thermal treatment. This ZnO layer subsequently served as both structural template and zinc precursor for the room-temperature aqueous conversion to ZIF-8 through ligand exchange (Fig. 1a). During the crystallization process, 2-MIM interacted with the ZnO layer and substituted the organic chains to form more stable ZIF-8 crystals (Fig. 1b). SEM analysis revealed distinct morphological evolution: pristine cotton fabrics exhibit smooth surfaces (Fig. 1c, left), while ZnO-deposited fabrics show dense arrays of rod-like nanostructures (Fig. 1c, center). Subsequent aqueous conversion yielded a continuous ZIF-8 coating comprising intergrown nanocrystals with uniform morphology and intimate substrate adhesion (Fig. 1c, right and S1d).

Compared with current synthesis route, our ambient aqueous synthesis represented an inexpensive and environmentally friendly approach. The process avoids the use of large complex equipment, expensive precursor, high-temperature or high-pressure conditions and organic solvents, making it more environmentally friendly and highly practical. By immersing the fabric in $Zn(CH_3COO)_2$ aqueous solution followed by thermal treatment, ZnO nanorods were uniformly generated on the surface of fabric, and overcame traditional limitations of heterogeneous nucleation and low loading content on polymeric substrates. This strategy utilizes ZnO nanorod-coated fabrics as dual-function

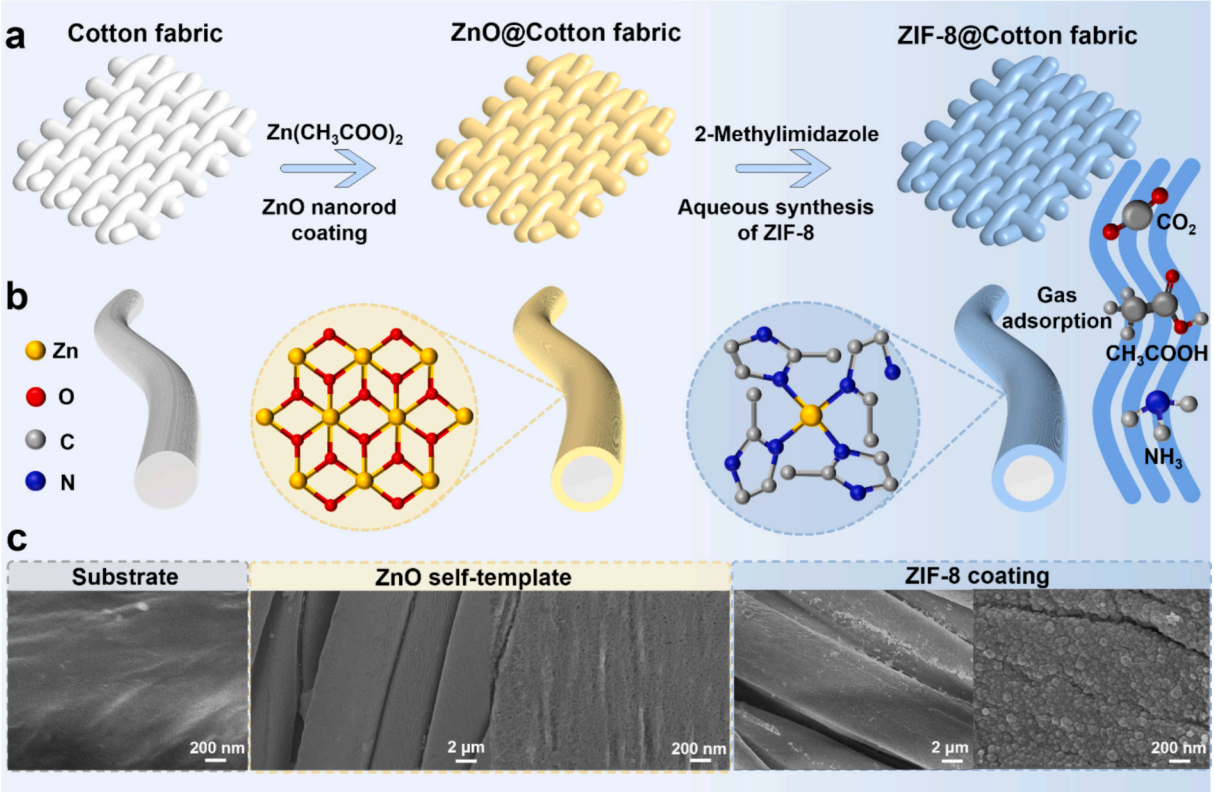

Fig. 1. ZIF-8 coated cotton fabrics from self-sacrificial ZnO templating and application for harmful gas adsorption. (a) Schematic of ZIF-8 coating formation process. (b) Schematic illustration and crystalline structure of ZnO and ZIF-8. Zn, O, C and N atoms are depicted in yellow, red, grey and blue, respectively. H atoms are not presented for clarity. (c) SEM images of fibrous substrate, ZnO self-template prepared with $Zn(CH_3COO)_2$ concentration of 20 wt% and corresponded synthesized ZIF-8 coating. (For interpretation of the references to colour in this figure legend, the reader is referred to the web version of this article.)

templates, which simultaneously provide self-supplied zinc precursors through a solid-state conversion and self-sacrificial template of structural guidance for crystal growth. The template-directed synthesis offers three significant advantages: (1) enhanced interfacial adhesion through ZnO-guided coordination, (2) simplified single-step synthesis eliminating external zinc sources, and (3) enhanced structural controllability through template-directed growth to facilitate uniform ZIF-8 crystals formation. The resulting composites demonstrated excellent crystalline integrity of coating while maintaining textile flexibility, which establishes a solid foundation for subsequent gas adsorption performance evaluation.

3.2. Control of ZIF-8 coating fabrication through precursor concentration regulation

The influence of $Zn(CH_3COO)_2$ precursor concentration (5, 10, 20, and 30 wt%) on ZnO template formation was systematically investigated. During thermal treatment at 130 °C for 2 h, ZnO layer formation preferentially occurred at the fabric-precursor interface through thermal decomposition (Fig. 2a). SEM revealed that ZnO layers exhibited a nanorod structure, with increasing precursor concentration inducing size reduction and layer densification (Fig. 2c and S1a). The morphology of ZnO nanorod prepared through solid-state conversion method was

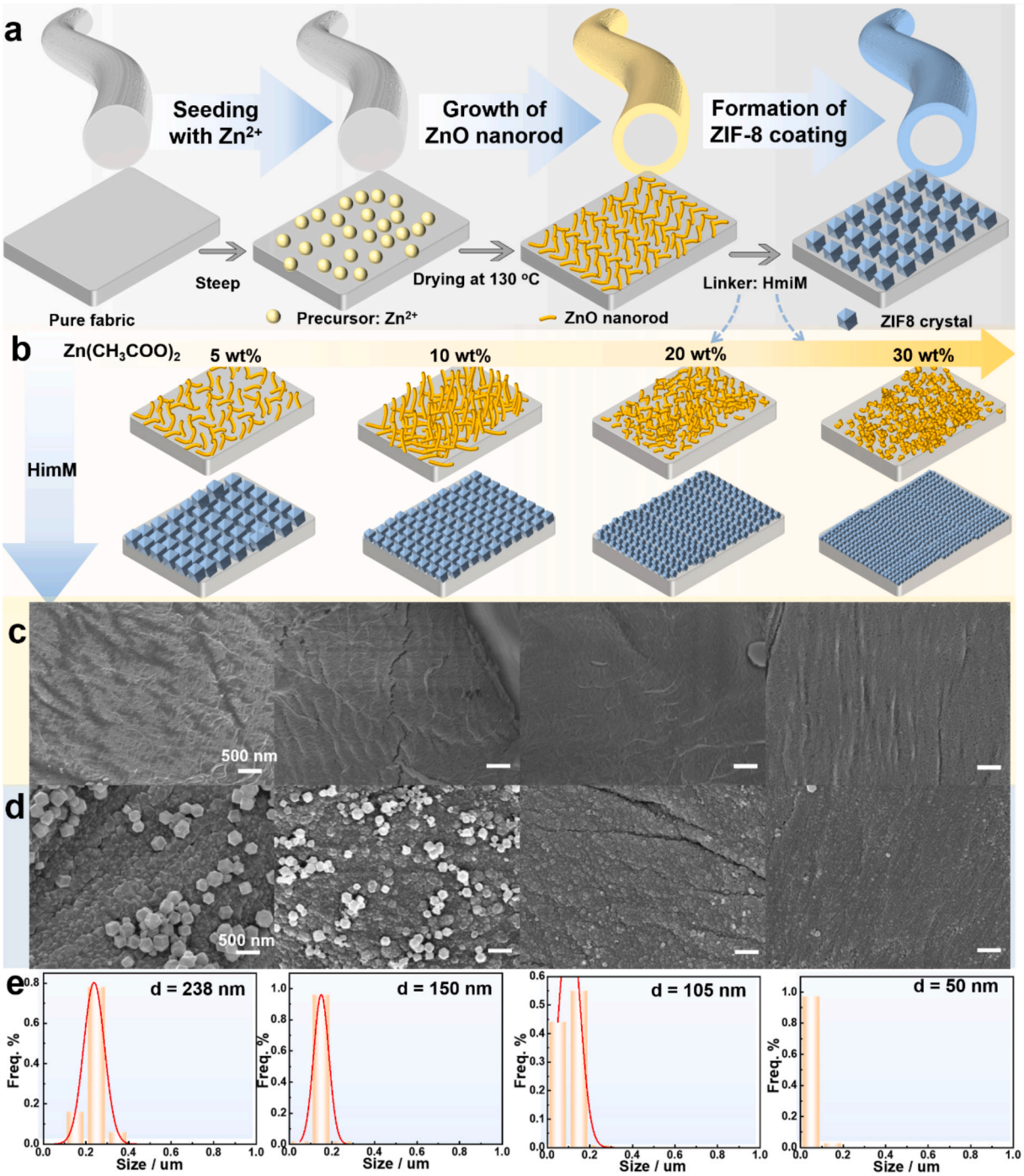

Fig. 2. (a) Schematic illustration of the preparation of the ZIF-8 coating on the cotton fabric and (b) the regulating the content and size of ZIF-8 by controlling the concentration of $Zn(CH_3COO)_2$. The concentration of $Zn(CH_3COO)_2$ from left to right was 5, 10, 20 and 30 wt%. SEM images of ZnO@cotton fabric (c) and ZIF8@cotton fabric (d). (e) The particle size statistical charts of corresponded ZIF-8 crystals on fabric.

effectively controlled by precursor concentration, reaction duration and temperature [35–37], and higher precursor concentrations resulted in densely packed nanostructured assemblies in our study (Fig. 2b). PXRD showed the diffraction peaks correspond to (100), (002) and (101) from ZnO@cotton fabric (precursor concentration of 20 wt% Zn^{2+}), which match in both position and relative intensity with the hexagonal ZnO standard (JCPDS 36–1451) (Fig. 3a). Therefore, the ZnO layer composed predominantly of randomly oriented ZnO nanorods, possibly imbedded in or associated with the cotton substrate (Fig. 2a and S1c).

Notably, the sacrificial ZnO layer was used to deliver the Zn^{2+} ions for initiation and support of ZIF-8 growth. The successful transformation from the ZnO layer to the ZIF-8 layer was carried out by immersion of the ZnO-coated substrates into the 2-MIM (linker component) aqueous solution at 25 °C for 4 h. Complete ZnO-to-ZIF-8 conversion was verified by 1) PXRD peak transitions (no characteristic peaks of $Zn(CH_3COO)_2$, and ZnO reflections replaced by ZIF-8 characteristic peaks at 7.5° (110), 10.4° (200), 12.8° (211)) (Fig. 3a and S3c), 2) FTIR spectral evolution (disappearance of ZnO-associated OH (3000–3500 cm^{-1}) and C═O (1545 cm^{-1}) vibrations, emergence of ZIF-8 characteristic peaks: C═N (1590 cm^{-1}), imidazolate ring bending (759–995 cm^{-1})) [15,25]

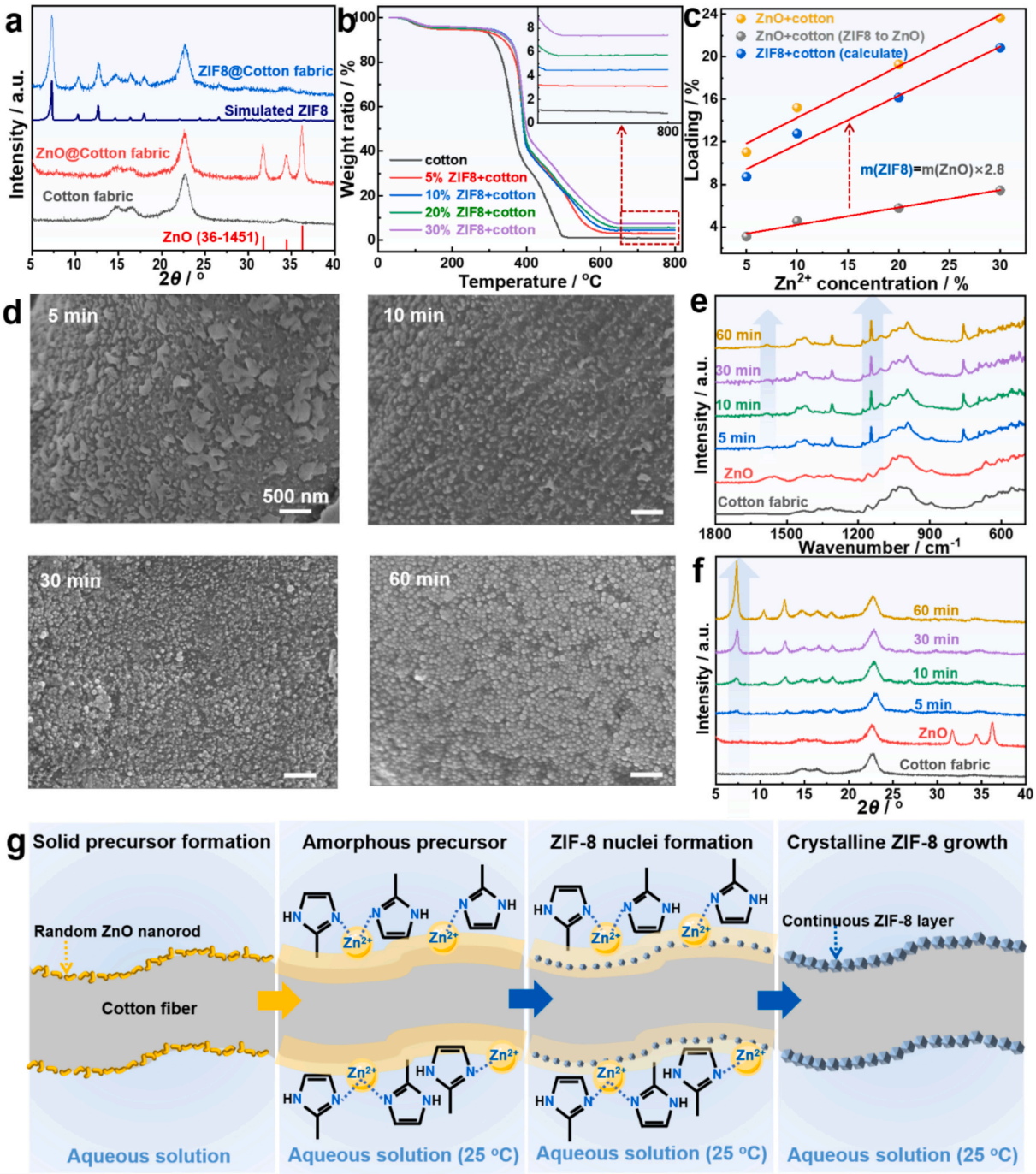

Fig. 3. (a) PXRD pattern of the simulated ZnO (JCPDS 36–1451), ZIF-8 and samples. (b) TGA curves of ZIF8@cotton fabric. (c) The contents and their corresponding correlation of ZnO and ZIF8 with the increase of $Zn(CH_3COO)_2$ concentration. (d) SEM images showing the changes on the cotton surface: pristine cotton fiber, ZnO@cotton fiber treated with 30 wt% $Zn(CH_3COO)_2$ and ligand treatment for 5, 10, 30 and 60 min. All scale bars are 500 nm. (e) PXRD patterns and (f) FTIR spectra of the corresponding samples. (g) Schematic illustration of the crystalline transition mechanism, where the yellow layer represents the amorphous precursor intermediates. (For interpretation of the references to colour in this figure legend, the reader is referred to the web version of this article.)

(Fig. S3a), 3) XPS analysis confirming Zn—N coordination (~1.3 eV positive shift in Zn $2p_{3/2}$ and $2p_{1/2}$) and ligand incorporation (new C-N/C=N bonds) [14] (Figs. S4 and 5).

Furthermore, TGA quantitatively revealed the concentration-dependent mass loading evolution from ZnO to ZIF-8 coatings while assessing their thermal stability. Pristine cotton substrates exhibited characteristic degradation profiles: 1) initial 2.6 ± 0.5% mass loss below 100 °C from moisture evaporation, and 2) large 96.7 ± 0.8% mass loss between 330 and 500 °C due to cellulose pyrolysis, ultimately leaving negligible residue (0.7 ± 0.1%) (Fig. 3b). ZnO-coated fabrics demonstrated exceptional thermal stability with <1% mass loss up to 800 °C, enabling precise ZnO quantification (11.02 to 23.63 wt%) proportional to precursor concentration (5 to 30 wt% Zn^{2+}) (Fig. S6). The ZIF-8@cotton system showed distinct thermal behavior, with complete framework decomposition above 550 °C ultimately yielding ZnO residues under the air atmosphere. Through stoichiometric analysis, the effective ZIF-8 loading increased from 8.71 to 20.83 wt% with rising precursor concentration (Fig. 3b and c), corroborated by progressive XRD peak intensification ((110) reflection) and FTIR signal enhancement (C=N vibration intensity) (Figs. S3b and d). Solvent selection critically influenced ZnO templating efficiency and subsequent ZIF-8 loading. Although alcoholic solutions (methanol/ethanol) produced continuous ZIF-8 coatings with ~50 nm crystallites, they achieved only 1.5 ± 0.3 wt% loading (Figs. S9 and 10). This limitation may be due to the reduced zinc acetate solubility in alcohols, and incomplete ZnO formation during drying. This templating approach has been successfully extended to diverse fabric substrates (e.g., flax and polyester), all yielding ZIF-8 coated fabrics with comparable efficacy, which effectively validates the methodology's general applicability (Figs. S8 and 11).

In addition to the mass loading regulation, systematic modulation of Zn^{2+} precursor concentration enabled precise control over ZIF-8 crystal morphology and dimensions. Increasing $Zn(CH_3COO)_2$ concentration in the steeping solution induced an obvious reduction in ZnO nanorod dimension while enhancing the denser layered structure (Fig. 2c and S1a). Subsequent conversion in 2-MIM aqueous solution revealed an inverse relationship between ZIF-8 crystal size and precursor concentration (Fig. 2d and S1b). Notably, the ZIF-8 content increased from 8.71 to 20.83 wt% loading (Fig. 3c) at 5 to 30 wt% Zn^{2+}, while the average ZIF-8 crystal size decreased from ~238 nm to ~50 nm (Fig. 2e and S7). The denser ZnO nanostructure with higher surface area promoted dissolution in the slightly alkaline 2-MIM solution (pH 8–9), releasing Zn^{2+} ions and creating a high-concentration microenvironment, which accelerated Zn^{2+}-2-MIM coordination and increasing ZIF-8 nucleation density. It can be concluded that the nucleation and growth of the ZIF-8 crystals are both restricted to the structure of ZnO self-sacrificing template. By regulating the $Zn(CH_3COO)_2$ concentration, the nucleation density of ZnO can be precisely controlled, which in turn determined the availability of zinc sources and reaction sites for ZIF-8 synthesis. This template-directed hierarchical architecture, where the primary nanostructure (ZnO) governs the secondary phase (ZIF-8), facilitates the fabrication of multifunctional fabrics with tunable surface properties.

3.3. Crystalline transition from ZnO to ZIF-8 through amorphous precursor intermediates

To study the ZnO-to-ZIF-8 transformation mechanism, we conducted time-resolved characterization of cotton fabrics immersed in 2-MIM aqueous solution using time-dependent SEM, PXRD and ATR-FTIR. SEM images revealed that small crystals with diameters below 100 nm and some microparticles with diameters about 500 nm formed on the substrate surface after 5 min of treatment in the 2-MIM solution. And after 10 min, the microparticles disappeared, leaving only small crystals on the surface (Fig. 3d). The PXRD pattern (Fig. 3f) showed that there were no distinct characteristic peaks of ZIF-8 after 5 min immersion. However, the FTIR spectra (Fig. 3e) showed obvious C—N and C=N stretching vibration (1148 and 1590 cm^{-1}), which means that the 2-MIM ligands begin to coordinate with Zn^{2+}. Therefore, combined with the results of PXRD and FTIR at 5 min immersion, the ZnO nanorod completely dissolved to release Zn^{2+}, and 2-MIM quickly coordinated with Zn^{2+} on the surface, which suggested the amorphous precursor formation. In fact, amorphous intermediate phases are often observed and integral to the crystalline process of ZIF-8 [38,39]. Recently, combining harmonic light scattering and static nuclear magnetic resonance (NMR), Dor et.al [40] have captured the crystallization mechanism of ZIF-8 in unprecedented detail. ZIF-8 nucleation fundamentally relies on an amorphous-to-crystalline transformation, transitioning from aggregated and ligand-rich prenucleation clusters to charge neutral amorphous precursors particles that ultimately crystallize. In the transient phase, Zn^{2+}-2 MIM complexes were observed in small nanoaggregates through static ^1H NMR. Our time-dependent PXRD (loss of crystallinity) and FTIR (emergence of Zn—N coordination bands) observations at 5 min align perfectly with the macroscopic signatures of this intermediate phase as reported in these fundamental studies.

Then, with prolonged immersion (10 min), the ZIF-8 characteristic peaks in the PXRD appeared and there were many small and uniform crystals on the surface in the SEM image, as a result of ZIF-8 nuclei formation. The ZIF-8 peaks in the PXRD pattern became stronger and sharper with increasing reaction time confirming the continuous growth of the ZIF-8 crystals. Finally, crystals with a stable diameter of approximately 50 nm formed after 60 min of reaction because of the exhaustion of the Zn^{2+} precursor (Fig. 3d and g). The results indicate that both precursor concentration and reaction time significantly influence the ZIF-8 mass loading and crystal size on the fabric. As shown in Fig. 3d and f, crystals grow progressively over time, with noticeable differences in size and loading observed between 30 min and 60 min. Growth approached completion after 60 min, justifying the selection of a 2-h reaction time. Importantly, the time-dependent PXRD analysis (Fig. 3a and f) reveals that the phase transition from ZnO to ZIF-8 proceeds with exceptionally high conversion. According to the methodological framework established by Kwon et al. [41], this is likely due to the high aspect ratio of the Zn template we employed and the sufficiently high ligand concentration, which prevent partial conversion on the surface and allow complete penetration of 2-MIM. Compared with other bulky or agglomerated solid zinc sources (which often leave residual cores), our ZnO nanorod strategy not only guarantees high phase conversion but also provides robust interfacial adhesion to the textile substrate, which ensure the mechanical durability of the final composite.

3.4. Manufacturing feasibility and stability optimization of ZIF-8 loaded fabrics

This facile and cost-effective synthetic strategy offers an environmentally friendly approach owing to its operation under room temperature conditions utilizing water as a green solvent alternative to conventional methanol or ethanol. Furthermore, this method exhibits high precursor conversion efficiency and shows promise for further scale-up. Its mild conditions could contribute to lower energy use and reduced waste. Fig. S12c shows cotton fabric samples measuring 15 cm × 25 cm with varied ZIF-8 mass loadings. Moreover, we successfully scaled up the preparation to 0.8 m × 0.8 m fabric (Fig. S15a). Powder XRD pattern (Fig. S15e) confirmed the successful preparation, TGA curve (Fig. S15d) showed a mass loading content of 18 wt%, and SEM images (Fig. S15b and c) revealed a dense ZIF-8 intergrown coating, which demonstrating the manufacturing feasibility of this aqueous route at a practical size. However, the transition from batch immersion to continuous manufacturing will require solutions for kinetic control and large-area uniformity. This work provides an eco-friendly foundation, but further engineering is needed to realize industrial application.

The enhanced hydrophobicity of ZIF-8 loaded fabrics, particularly with reduced particle sizes, arises from synergistic surface roughness effects and intrinsic hydrophobic structure of conjugated imidazolate

rings [42] [43]. Smaller ZIF-8 particles enabled denser fiber coverage and lower coating defect density, forming continuous hydrophobic barriers as evidenced by water contact angles increasing from 92° to 131° (Fig. 4c). Despite the ambient synthesis and subsequent drying at 130 °C, the coated fabrics successfully retained over 90% of their pristine breaking strength and elongation at break in both the longitudinal (Fig. 4d) and latitudinal (Fig. S12e) directions, demonstrating the exceptional mechanical stability of the composite.

Moisture management capabilities were preserved with water vapor transmission rates (WVTR) showing only 8.2 ± 0.5% reduction, confirming the non-occlusive nature of the microporous coating (Fig. 4b). Although the in-situ growth strategy effectively eliminates the inhalation risk of physical MOF shedding, the application of Zn-based MOFs in personal protective equipment still necessitates careful consideration of chemical degradation when exposure to physiological humidity or sweat [44]. Washing durability tests revealed 3 wt% mass loss after accelerated laundering (equivalent to three standard domestic wash cycles (Fig. 4a)) with TGA confirming (Fig. S12d). Despite some loss of coating, it is noteworthy that the intergrown ZIF-8 crystal layer remained largely unaffected, as evidenced by SEM images (Fig. S12b). This observation demonstrated the structural and morphological stability of the ZIF-8 coated fabrics, mainly attributed to the strong interfacial interactions

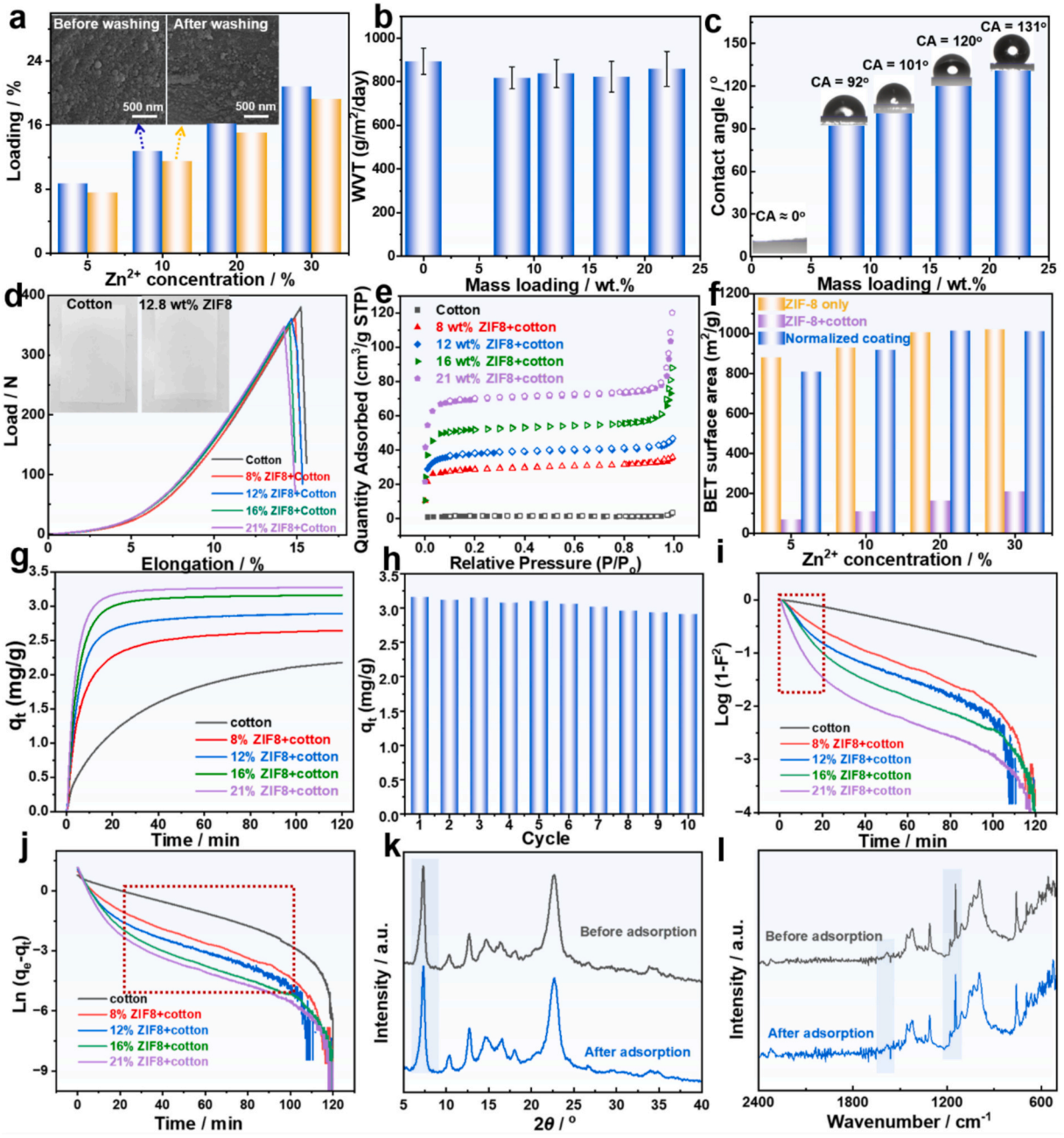

Fig. 4. (a) The comparison of loading content of ZIF-8 crystal before and after the washing. The insets are the SEM images ZIF-8@cotton fabric before and after the washing. (b) Water vapor transmission rates values of the samples. (c) Contact angle photograph of corresponded samples. (d) Load-elongation curves of cotton and scaled-up ZIF-8@cotton samples from longitudinal direction. The insets are the photographs of scaled-up (15 cm × 25 cm) with 12.8 wt% ZIF-8 coating on the cotton fabric. (e) N_2 adsorption isotherm of the prepared ZIF-8@cotton. (f) The BET surface area values of ZIF-8 powder, ZIF-8@cotton and normalized ZIF-8 coatings. (g) Time effect on the adsorption quantity of ammonia onto the different samples (2.0 g) at room temperature and adsorption cycles of ammonia on 16 wt% ZIF-8-coated cotton (h). Adsorption diffusion kinetic models (D—W model) (i) and reaction kinetic models (PFO model) (j) of ammonia onto the samples. PXRD pattern (k) and FTIR spectra (l) of 16 wt% ZIF-8 coated cotton before and after ammonia adsorption.

between constituent phases, which suggests potential for extended service life in applications requiring repeated mechanical/chemical stress resistance.

3.5. Harmful gas adsorption properties of ZIF-8 loaded fabrics

MOF-incorporated composite fabrics have emerged as next-generation solutions for harmful gas mitigation, demonstrating potential applications ranging from personal protective equipment to gas purification systems [3,45,46]. Nitrogen adsorption at 77 K revealed the porous characteristics of both ZIF-8 powder and composite fabrics (Fig. 4e and S13a). Enhanced precursor concentrations resulted in increased ZIF-8 loading and reduced crystal size, leading to greater porosity in coated fabrics. The Brunauer-Emmett-Teller (BET) surface area of ZIF-8 powder increased from 882.8 to 1021.8 m^2/g with higher precursor concentrations, while composite materials showed a corresponding increase from 70.5 to 210.9 m^2/g (Fig. 4f). Notably, when normalized by ZIF-8 mass loading, the calculated BET surface area of the ZIF-8 component ranged from 808.5 to 1012.4 m^2/g, consistent with values obtained for ZIF-8 powder synthesized from aqueous Zn^{2+} precursor solutions.

The microporous structure of ZIF-8 enables CO_2 adsorption through Langmuir-type binding sites which can be replaced by CO_2 molecules [8]. This prompted investigation of ZIF-8@cotton composites for CO_2 capture. Complete CO_2 adsorption isotherms at 298 K up to 1 bar demonstrated that pure ZIF-8 powder achieved exceptional gas uptake (26.8 to 30.5 cm^3/g at 1 bar), while ZIF-8@cotton composites maintained significant adsorption capacity (2.9 to 5.6 cm^3/g at 1 bar), confirming accessible active sites in the composite system (Fig. S13b and c). Cyclic adsorption-desorption testing of five cycles revealed fully reversible CO_2 adsorption with negligible capacity loss (Fig. S13d).

Ammonia and acetic acid are representative harmful gases that have raised widespread public concern due to their detrimental effects [12,45,47–49]. Owing to its facile synthesis, low cost, and exceptional ammonia stability derived from nitrogen-donor linkers, ZIF-8 is positioned as an ideal material for ammonia adsorption [50,51]. And the microporous structure of ZIF-8 also provide enough active Langmuir-type bonding sites for the adsorption of acetic acid [52]. Dynamic adsorption studies of ammonia and acetic acid in sealed systems at room temperature and pressure (RTP) demonstrated superior performance of ZIF-8 composites (Fig. S13e and f) [33,34,53]. Ammonia concentration decreased to near-zero levels within 120 min for composites with optimal ZIF-8 loading (20.8 wt%), compared to residual 15.2 mg/L for pure cotton. The 20.8 wt% ZIF-8@cotton fabric exhibited the fastest adsorption kinetics and highest ammonia uptake. The enhanced gas adsorption performance may be attributed to a synergistic effect from optimized precursor concentration: higher mass loading provides more active sites, smaller crystal size minimizes diffusion resistance, and continuous coverage ensures maximal contact. To decouple crystal size from mass loading, we synthesized control samples with identical loading (~8 wt%) but different crystal sizes. By substituting water with methanol during in-situ growth, we altered nucleation kinetics to obtain ultra-small ZIF-8 crystals (~60 nm) without changing the final loading, which were compared against larger crystals (~238 nm) at the same 8 wt%. Ammonia adsorption curves (Fig. S16) show that the ~60 nm sample exhibits significantly higher capacity than the ~238 nm sample. This decoupled comparison definitively proves that, independent of mass loading, reducing crystal size inherently enhances adsorption performance by increasing the effective surface area. In addition, acetic acid adsorption showed slightly reduced efficiency, with final concentrations reaching 16.8 mg/L versus 53.2 mg/L for untreated cotton. The adsorption quantity (q_t) of ammonia and acetic acid onto the samples with contact time (t) was shown in Fig. 4g and S13g. It can be observed that ZIF-8 coated cotton fabrics has better ammonia adsorption quantity than acetic acid (3.3 mg/g vs. 2.5 mg/g as for 20.8 wt% ZIF-8 coated cotton). Therefore, we choose the ammonia adsorption to further study the corresponded adsorption kinetic.

Adsorption kinetics for ammonia on the original cotton and ZIF-8 coated cotton was studied to predict equilibrium adsorption capacity for odor control. Given rapid gas circulation eliminated mass transfer effects, two diffusion models (Dumwald-Wagner and Weber-Morris) and two reaction models (Pseudo-first-order and Pseudo-second-order) were applied to analyze adsorption mechanisms [33]. Fig. 4i and S13h shows the diffusion kinetic model (D—W model and W-M model) plot, and Fig. 4j and S13i shows the reaction kinetic model (PFO model and PSO model) plot for ammonia removal with five fabrics under the same condition. Adsorption kinetics of ammonia on five fabrics revealed distinct mechanisms across time ranges. In the initial 20 min, diffusion models (D—W and W-M) dominated (higher R^2), indicating intraparticle diffusion control. Beyond 20 min, R^2 for diffusion models declined, while the PFO and PSO model showed superior fit, suggesting adsorption shifted to surface site occupation. As shown in Table S1, calculated equilibrium capacities ($q_{e.cal}$) from PFO closely matched experimental values ($q_{e.exp}$). Initial adsorption rates (h_2) increased with the increase of loading content of ZIF-8, implying 20.8 wt% ZIF-8 coated cotton fabric had the most active binding sites for ammonia [34,54].

Results of PXRD pattern and FTIR spectra of ZIF-8 coated cotton fabric before and after ammonia adsorption are shown in Fig. 4k and l. The PXRD and FTIR spectra before and after ammonia adsorption exhibited no significant changes in characteristic peaks, and no new peaks emerged, indicating the absence of chemical adsorption. However, prolonged exposure in ammonia (beyond 8 h) may cause substantial structural degradation of the ZIF-8 framework [51,55]. Although the long-term structural degradation is an undeniable physicochemical reality, the ZIF-8 framework exhibits sufficient robustness for short-to-medium-term capture within our designed operational window (2 h). Therefore, explore advanced surface passivation strategies to enhance the ultra-long-term stability of ZIF-8 under continuous ammonia exposure will be a key focus of our subsequent research. Furthermore, the regeneration performance of the 16 wt% ZIF-8 coated fabric was systematically evaluated over 10 consecutive cycles. Following each adsorption experiment, the sample was fully desorbed and regenerated in a vacuum oven at 100 °C for 4 h. As depicted in Fig. 4h, the composite retained 90% of its initial capacity after the 10th cycle. The slight decrease in capacity results from the strong interactions between ammonia and ZIF-8 framework, which partially weakened metal/ligand bonds at its exposed surface, and inevitably leading to partial structural degradation of the framework during repeated thermal and chemical cycling [51]. And the adsorption curves for ammonia and acetic acid were measured on the 20.8 wt% ZIF-8 coated cotton fabric sample before and after washing. As shown in Fig. S14, its gas adsorption capacity remained virtually unchanged following the washing process. While this dynamic adsorption results provide a fundamental feasibility for the capture of harmful gases, translating this material into practical protective equipment will necessitate further rigorous evaluations, including breakthrough testing and competitive multi-gas environments, which will be the focus of our future studies.

4. Conclusion

A facile, scalable, and ambient aqueous synthesis method was developed to fabricate continuous ZIF-8 coated fabrics at an ambient temperature, advancing the performance of MOF-based flexible composite in harmful gas adsorption. Firstly, we have proposed a scalable approach on the preparation of ZIF-8 coating, which includes a solid-state method to prepare a self-sacrificial ZnO template, and then converts the template to ZIF-8 coating through ambient aqueous synthesis. By precisely regulating $Zn(CH_3COO)_2$ concentrations, we achieved controlled growth of randomly aligned ZnO nanorods array on fabric surfaces, which subsequently served as both sacrificial metal sources and structural templates for ZIF-8 crystallization. After the synthesis in the 2-MIM aqueous solution at room temperature, dense ZIF-8 coatings

with tunable crystal sizes (238 to 50 nm) and loading contents (8.7 to 20.8 wt%) were formed, which demonstrated a controllable preparation process. ZIF-8 coated fabrics on various substrates (such as flax and polyester) were also produced through this approach, demonstrating its broad applicability. This method eliminated harsh conditions and organic solvents, and overcame traditional limitations of heterogeneous nucleation and low loading content on polymeric substrates. Secondly, we have carried out an investigation into the mechanism of this green synthesis route. The crystalline transition from ZnO to ZIF-8 through amorphous precursor intermediates after immersing into the ligand solution. Finally, we have investigated the stability and gas adsorption properties of the materials. The prepared large-scaled samples revealed good mechanical strength, laundering durability, and moisture permeability. Gas adsorption experiments demonstrated excellent removal efficiencies for NH_3 (3.3 mg/g at RTP), CH_3COOH (2.5 mg/g at RTP) and CO_2 (5.6 cm^3/g at 1 bar) contaminants through active binding sites. This approach offers a sustainable route that incorporates MOF coating on fabrics, and the resulting fabrics exhibit promising functionality for human health and environmental sustainability, especially for personal protective equipment, where efficient adsorption of harmful gases is essential.

Declaration of competing interest

The authors declare that they have no known competing financial interests or personal relationships that could have appeared to influence the work reported in this paper.

Acknowledgements

The work described in this paper was supported by a grant from the Joint Research Centre for Fiber Innovations and Renewable Materials (P0053922), Research Grants Council (GRF grants No. 15209623 and 15304125) of the Hong Kong Special Administrative Region. We also acknowledge the support from the start-up fund of the Hong Kong Polytechnic University (1-BDD2), HKPM-PolyU Joint Chinese Textile Centre (1-5Y13), and Research Institute for Intelligent Wearable Systems (1-CDPY).

Appendix A. Supplementary data

Supplementary data to this article can be found online at https://doi.org/10.1016/j.seppur.2026.138152.

Data availability

Data will be made available on request.

References

[1] Z. Zhou, T. Ma, H. Zhang, S. Chheda, H. Li, K. Wang, S. Ehrling, R. Giovine, C. Li, A. H. Alawadhi, M.M. Abduljawad, M.O. Alawad, L. Gagliardi, J. Sauer, O.M. Yaghi, Carbon dioxide capture from open air using covalent organic frameworks, Nature 635 (2024) 96–101.
[2] Q. Qian, P.A. Asinger, M.J. Lee, G. Han, K. Mizrahi Rodriguez, S. Lin, F. M. Benedetti, A.X. Wu, W.S. Chi, Z.P. Smith, MOF-based membranes for gas separations, Chem. Rev. 120 (2020) 8161–8266.
[3] G.W. Peterson, D.T. Lee, H.F. Barton, T.H. Epps, G.N. Parsons, Fibre-based composites from the integration of metal–organic frameworks and polymers, Nat. Rev. Mater. 6 (2021) 605–621.
[4] D.T. David Britt, Omar M. Yaghi, Metal-organic frameworks with high capacity and selectivity for harmful gases, Proc. Natl. Acad. Sci. 105 (2008) 11623–11627.
[5] S. Shi, W. Bai, X. Chen, Y. Si, C. Zhi, H. Wu, Y. Su, W. Cai, B. Fei, C.W. Kan, J. Hu, X. Wang, Advances in Nanofiber Filtration Membranes: From Principles to Intelligent Applications, Adv. Funct, Mater, 2025.
[6] S. Bose, D. Sengupta, T.M. Rayder, X. Wang, K.O. Kirlikovali, A.K. Sekizkardes, T. Islamoglu, O.K. Farha, Challenges and Opportunities: Metal–Organic Frameworks for Direct Air Capture, Adv. Funct. Mater. 34 (2023).
[7] L. Yang, X. Cui, Z. Zhang, Q. Yang, Z. Bao, Q. Ren, H. Xing, An asymmetric anion-pillared metal-organic framework as a multisite adsorbent enables simultaneous removal of propyne and propadiene from propylene, Angew. Chem. Int. Ed. 57 (2018) 13145–13149.
[8] X. Gong, Y. Wang, T. Kuang, ZIF-8-based membranes for carbon dioxide capture and separation, ACS Sustain. Chem. Eng. 5 (2017) 11204–11214.
[9] M. Tu, S. Wannapaiboon, K. Khaletskaya, R.A. Fischer, Engineering Zeolitic-Imidazolate framework (ZIF) thin film devices for selective detection of volatile organic compounds, Adv. Funct. Mater. 25 (2015) 4470–4479.
[10] K. Ma, Y.H. Cheung, K.O. Kirlikovali, H. Xie, K.B. Idrees, X. Wang, T. Islamoglu, J. H. Xin, O.K. Farha, Fibrous Zr-MOF nanozyme aerogels with macro-Nanoporous structure for enhanced catalytic hydrolysis of organophosphate toxins, Adv. Mater. 36 (2023).
[11] K. Ma, K.B. Idrees, F.A. Son, R. Maldonado, M.C. Wasson, X. Zhang, X. Wang, E. Shehayeb, A. Merhi, B.R. Kaafarani, T. Islamoglu, J.H. Xin, O.K. Farha, Fiber Composites of Metal–Organic Frameworks, Chem. Mater. 32 (2020) 7120–7140.
[12] S. Bose, D. Sengupta, X. Wang, C.S. Smoljan, J.J. Mahle, J.A. Tokarz, T.M. Rayder, K. Ma, K.O. Kirlikovali, T. Islamoglu, G.W. Peterson, O.K. Farha, Development of a multiparticulate metal-organic framework/textile fiber swatch, ACS Appl. Mater. Interfaces 17 (2025) 17813–17822.
[13] K. Ma, T. Islamoglu, Z. Chen, P. Li, M.C. Wasson, Y. Chen, Y. Wang, G.W. Peterson, J.H. Xin, O.K. Farha, Scalable and Template-Free Aqueous Synthesis of Zirconium-Based Metal–Organic Framework Coating on Textile Fiber, J. Am. Chem. Soc. 141 (2019) 15626–15633.
[14] H. Singh Jhinjer, M. Jassal, A.K. Agrawal, Metal-organic frameworks functionalized cellulosic fabrics as multifunctional smart textiles, Chem. Eng. J. 478 (2023).
[15] K. Ma, Z. Chen, T. Islamoglu, C. Lai, X. Wang, B. Fei, O.K. Farha, J.H. Xin, Facile and scalable coating of metal−organic frameworks on fibrous substrates by a coordination replication method at room temperature, ACS Appl. Mater. Interfaces 11 (2019) 22714–22721.
[16] R. Cao, Z. Chen, Y. Chen, K.B. Idrees, S.L. Hanna, X. Wang, T.A. Goetjen, Q. Sun, T. Islamoglu, O.K. Farha, Benign integration of a Zn-Azolate metal-organic framework onto textile fiber for ammonia capture, ACS Appl. Mater. Interfaces 12 (2020) 47747–47753.
[17] K. Khaletskaya, S. Turner, M. Tu, S. Wannapaiboon, A. Schneemann, R. Meyer, A. Ludwig, G. Van Tendeloo, R.A. Fischer, Self-directed localization of ZIF-8 thin film formation by conversion of ZnO nanolayers, Adv. Funct. Mater. 24 (2014) 4804–4811.
[18] J.C. Tan, T.D. Bennett, A.K. Cheetham, Chemical structure, network topology, and porosity effects on the mechanical properties of zeolitic imidazolate frameworks, Proc. Natl. Acad. Sci. 107 (2010) 9938–9943.
[19] F. Dorosti, L. Ge, H. Wang, J. Bell, R. Lin, J. Hou, Z. Zhu, Non-selective defect minimization towards highly efficient metal-organic framework membranes for gas separation, Angew. Chem. Int. Ed. 64 (2024).
[20] Y. Li, C. Ma, P. Nian, H. Liu, X. Zhang, Green synthesis of ZIF-8 tubular membranes from a recyclable 2-methylimidazole water-solvent solution by ZnO nanorods self-converted strategy for gas separation, J. Membr. Sci. 581 (2019) 344–354.
[21] H.S. Jhinjer, A. Singh, S. Bhattacharya, M. Jassal, A.K. Agrawal, Metal-organic frameworks functionalized smart textiles for adsorptive removal of hazardous aromatic pollutants from ambient air, J. Hazard. Mater. 411 (2021) 125056.
[22] J. Zhao, W.T. Nunn, P.C. Lemaire, Y. Lin, M.D. Dickey, C.J. Oldham, H.J. Walls, G. W. Peterson, M.D. Losego, G.N. Parsons, Facile Conversion of Hydroxy Double Salts to Metal–Organic Frameworks Using Metal Oxide Particles and Atomic Layer Deposition Thin-Film Templates, J. Am. Chem. Soc. 137 (2015) 13756–13759.
[23] M. Bechelany, M. Drobek, C. Vallicari, A. Abou Chaaya, A. Julbe, P. Miele, Highly crystalline MOF-based materials grown on electrospun nanofibers, Nanoscale 7 (2015) 5794–5802.
[24] P.K. Xiaoli Ma, Nitish Mittal, Alexandra Khlyustova, Prodromos Daoutidis, K. Andre Mkhoyan, Michael Tsapatsis, Zeolitic imidazolate framework membranes made by ligand-induced permselectivation, Science 361 (2018) 1008–1011.
[25] W. Li, P. Su, Z. Li, Z. Xu, F. Wang, H. Ou, J. Zhang, G. Zhang, E. Zeng, Ultrathin metal-organic framework membrane production by gel-vapour deposition, Nat. Commun. 8 (2017) 406.
[26] Y. Yuan, H. Wu, H. Lu, Y. Zheng, J.Y. Ying, Y. Zhang, ZIF nano-dagger coated gauze for antibiotic-free wound dressing, Chem. Commun. 55 (2019) 699–702.
[27] J.H. Lee, D. Kim, H. Shin, S.J. Yoo, H.T. Kwon, J. Kim, Zeolitic imidazolate framework ZIF-8 films by ZnO to ZIF-8 conversion and their usage as seed layers for propylene-selective ZIF-8 membranes, J. Ind. Eng. Chem. 72 (2019) 374–379.
[28] Y. Wang, Y. Ge, R. Wang, Z. Liu, Z. Yin, Z. Yang, F. Liu, W. Yang, MOF-derived Ni/ZIF-8/ZnO arrays on carbon fiber cloth for efficient adsorption-catalytic oxidation, Small 19 (2023) e2303928.
[29] A. Huang, H. Bux, F. Steinbach, J. Caro, Molecular-sieve membrane with hydrogen permselectivity: ZIF-22 in LTA topology prepared with 3-aminopropyltriethoxysilane as covalent linker, Angew. Chem. Int. Ed. 49 (2010) 4958–4961.
[30] C. Liu, Y.N. Wu, C. Morlay, Y. Gu, B. Gebremariam, X. Yuan, F. Li, General deposition of metal-organic frameworks on highly adaptive organic-inorganic hybrid electrospun fibrous substrates, ACS Appl. Mater. Interfaces 8 (2016) 2552–2561.
[31] Y. Chen, S. Zhang, S. Cao, S. Li, F. Chen, S. Yuan, C. Xu, J. Zhou, X. Feng, X. Ma, B. Wang, Roll-to-roll production of metal-organic framework coatings for particulate matter removal, Adv. Mater. 29 (2017).
[32] S.A. Abdulla, R. Sabouni, M. Ghommem, A.H. Alami, ZIF-8 coated flexible carbon cloth substrates for CO_2 sensing applications, Appl. Surf. Sci. Adv. 18 (2023).
[33] W. Bai, H. Yu, L. Liu, E. Pakdel, B. Tang, H. Su, C. Hurren, L. Liu, J. Wang, X. Wang, The adsorption kinetics and mechanism of odorous gases onto textile fibers, RSC Sustainability 1 (2023) 357–367.

[34] W. Tang, J. Wang, W. Bai, R. Rajkhowa, D. Li, B. Tang, X. Wang, W. Xu, Fine powders from dyed waste wool as odor adsorbent and coloration pigment, Powder Technol. 400 (2022).
[35] X. Bulliard, S. Yun, S.-G. Ihn, Y.S. Choi, Y. Kim, D. Choi, J.-Y. Choi, W. Choi, Density control of ZnO nanorod arrays on mixed self-assembled monolayers, Cryst. Growth Des. 10 (2010) 4697–4700.
[36] S. Wang, Y. Yang, J. Chai, K. Zhu, X. Jiang, Z. Du, Nanoimprint assisted transfer of different density vertically aligned ZnO nanorod arrays, RSC Adv. 6 (2016) 64332–64337.
[37] Q. Li, J. Bian, J. Sun, J. Wang, Y. Luo, K. Sun, D. Yu, Controllable growth of well-aligned ZnO nanorod arrays by low-temperature wet chemical bath deposition method, Appl. Surf. Sci. 256 (2010) 1698–1702.
[38] J. Cravillon, C.A. Schröder, R. Nayuk, J. Gummel, K. Huber, M. Wiebcke, Fast nucleation and growth of ZIF-8 nanocrystals monitored by time-resolved in situ small-angle and wide-angle X-ray scattering, Angew. Chem. Int. Ed. 50 (2011) 8067–8071.
[39] R. Jain, A.J. Mallette, J.D. Rimer, Controlling nucleation pathways in zeolite crystallization: seeding conceptual methodologies for advanced materials design, J. Am. Chem. Soc. 143 (2021) 21446–21460.
[40] A.R. Dok, S. Radhakrishnan, F. de Jong, E. Becquevort, O. Deschaume, C. V. Chandran, Y. de Coene, C. Bartic, M. Van der Auweraer, W. Thielemans, C. Kirschhock, M.A. van der Veen, T. Verbiest, E. Breynaert, S. Van Cleuvenbergen, Amorphous-to-crystalline transformation: how cluster aggregation drives the multistep nucleation of ZIF-8, J. Am. Chem. Soc. 147 (2025) 8455–8466.
[41] M.K. Ohchan Kwon, Eunji Choi, Jun Hyuk Bae, Sungmi Yoo, Jong Chan Won, Yun Ho Kim, Ju Ho Shin, Jong Suk Lee, Dae Woo Kim, High–aspect ratio zeolitic imidazolate framework (ZIF) nanoplates for hydrocarbon separation membranes, Sci. Adv. 8 (2022) eabl6841.
[42] E.E. Sann, Y. Pan, Z. Gao, S. Zhan, F. Xia, Highly hydrophobic ZIF-8 particles and application for oil-water separation, Sep. Purif. Technol. 206 (2018) 186–191.
[43] A.U. Ortiz, A.P. Freitas, A. Boutin, A.H. Fuchs, F.X. Coudert, What makes zeolitic imidazolate frameworks hydrophobic or hydrophilic? The impact of geometry and functionalization on water adsorption, Phys. Chem. Chem. Phys. 16 (2014) 9940–9949.
[44] T.V. Tran, H.H. Dang, H. Nguyen, N.T.T. Nguyen, D.H. Nguyen, T.T.T. Nguyen, Synthesis methods, structure, and recent trends of ZIF-8-based materials in the biomedical field, Nanoscale. Adv. 7 (2025) 3941–3960.
[45] X. Song, Y. Wang, C. Wang, X. Gao, Y. Zhou, B. Chen, P. Li, Self-healing hydrogen-bonded organic frameworks for low-concentration ammonia capture, J. Am. Chem. Soc. 146 (2024) 627–634.
[46] X. Wang, H. Xie, D. Sengupta, F. Sha, K.I. Otake, Y. Chen, K.B. Idrees, K. O. Kirlikovali, F.A. Son, M. Wang, J. Ren, J.M. Notestein, S. Kitagawa, O.K. Farha, Precise modulation of CO_2 sorption in Ti_8Ce_2-Oxo clusters: elucidating Lewis acidity of the ce metal sites and structural flexibility, J. Am. Chem. Soc. 146 (2024) 15130–15142.
[47] C. Marsh, X. Han, J. Li, Z. Lu, S.P. Argent, I. da Silva, Y. Cheng, L.L. Daemen, A. J. Ramirez-Cuesta, S.P. Thompson, A.J. Blake, S. Yang, M. Schroder, Exceptional packing density of ammonia in a dual-functionalized metal-organic framework, J. Am. Chem. Soc. 143 (2021) 6586–6592.
[48] K.O. Kirlikovali, Z. Chen, X. Wang, M.R. Mian, S. Alayoglu, T. Islamoglu, O. K. Farha, Investigating the influence of hexanuclear clusters in isostructural metal-organic frameworks on toxic gas adsorption, ACS Appl. Mater. Interfaces 14 (2022) 3048–3056.
[49] Y. Zhang, X. Zhang, Z. Chen, K.I. Otake, G.W. Peterson, Y. Chen, X. Wang, L. R. Redfern, S. Goswami, P. Li, T. Islamoglu, B. Wang, O.K. Farha, A flexible interpenetrated zirconium-based metal-organic framework with high affinity toward ammonia, ChemSusChem 13 (2020) 1710–1714.
[50] Z. Liu, R. Cheng, J. Kim, S. Li, Ammonia adsorption performance of zeolitic imidazolate frameworks for cooling, Langmuir 39 (2023) 14726–14736.
[51] E. Choi, S. Yu, T. Kim, Y. Ji, M.H. Jeong, M. Kim, M. Park, K. Eum, K.C. Kim, D. W. Kim, Ammonia-induced metal–organic framework membrane pore tuning for hydrogen separation, Angew. Chem. Int. Ed. 65 (2026) e2261249.
[52] M. Amidi, E. Salehi, ZIF-8 derived porous carbon/ZnO as an effective nanocomposite adsorbent for removal of acetic acid, Korean J. Chem. Eng. 40 (2023) 2384–2395.
[53] X. Zhu, Y. Li, W. Tang, Y. Cui, K. Zhu, B. Zeng, J. Wang, X. Wang, Wool powder assisted colorimetric sensing yarn with high sensitivity for NH_3 monitoring, Biosens. Bioelectron. 267 (2025) 116833.
[54] G. An, X. Xia, S. Wu, Z. Liu, L. Wang, S. Li, Metal-organic frameworks for Ammonia-based thermal energy storage, Small 17 (2021) e2102689.
[55] H. Ji, W. Choi, E. Choi, Y. Ji, M. Kim, H.-J. Jeon, D.W. Kim, Degradation of polycrystalline zeolitic imidazolate framework membrane under reactive plasma conditions, J. Membr. Sci. Lett. 5 (2025).